Experimental investigation of surface determination process on multi-material components for dimensional computed tomography

Borges de Oliveira, Fabrício; Stolfi, Alessandro; Bartscher, Markus; De Chiffre, Leonardo

Published in:
Case Studies in Nondestructive Testing and Evaluation

Link to article, DOI:
10.1016/j.csndt.2016.04.003

Publication date:
2016

Document Version
Peer reviewed version

Accepted Manuscript

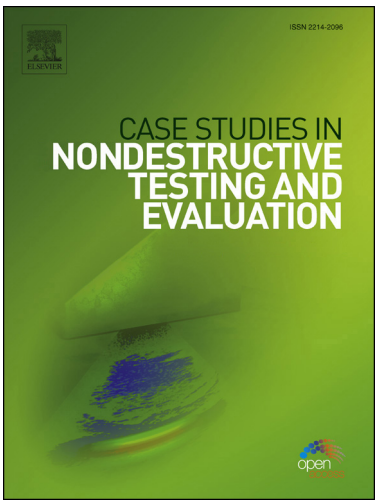

Experimental investigation of surface determination process on multi-material components for dimensional computed tomography

Fabrício Borges de Oliveira, Alessandro Stolfi, Markus Bartscher, Leonardo De Chiffre, Ulrich Neuschaefer-Rube

PII: S2214-6571(16)30008-9
DOI: http://dx.doi.org/10.1016/j.csndt.2016.04.003
Reference: CSNDT 33

To appear in: *Case Studies in Nondestructive Testing and Evaluation*

Please cite this article in press as: Borges de Oliveira F, et al. Experimental investigation of surface determination process on multi-material components for dimensional computed tomography. *Case Stud Nondestruct Test Eval* (2016), http://dx.doi.org/10.1016/j.csndt.2016.04.003

Highlights

- Investigation of surface determination process on multi-material CT measurements
- Measurements of step gauge-shaped multi-material assemblies
- Evaluation of 7 segmentation processes in Volume Graphics VGStudio Max 2.2.6

Experimental Investigation of Surface Determination Process on Multi-material Components for Dimensional Computed Tomography

Fabrício Borges de Oliveira[1] (corresponding author), Alessandro Stolfi[2], Markus Bartscher[1], Leonardo De Chiffre[2], Ulrich Neuschaefer-Rube[1]

[1]Physikalisch-Technische Bundesanstalt (PTB), Bundesallee 100, 38116 Braunschweig, Germany

e-mail: fabricio.borges@ptb.de, markus.bartscher@ptb.de, ulrich.neuschaefer-rube@ptb.de

[2]Technical University of Denmark (DTU), Produktionstorvet Building 425, Room 209, 2800 Kgs. Lyngby, Denmark

e-mail: alesto@mek.dtu.dk, ldch@mek.dtu.dk

Abstract

The possibility of measuring multi-material components, while assessing inner and outer features simultaneously makes X-ray computed tomography (CT) the latest evolution in the field of coordinate measurement systems (CMSs).
However, the difficulty in selecting suitable scanning parameters and suitable surface determination settings, limits a better acceptance of CT as a CMS. Moreover, standard CT users are subject to the algorithms and boundary conditions implied by the use of commercial analysis software.
In this context, this paper is concerned with the experimental evaluation of the influence of surface determination process on multi-material measurements, using functions available in the commercial CT data analysis software Volume Graphics VGStudio Max 2.2.6.
Calibrated step gauges made of different materials, i.e. PEEK, PPS, and Al were used as reference standards. The step gauges were assembled in such a way as to have different multi-material X-ray absorption ratios. Comparative measurements of mono-material assemblies were performed as well. Different segmentation processes were considered (e.g. ISO-50%, local threshold, region growing, etc.), patch-based bidirectional length analyses were carried out to perform in-material measurements on the assemblies.
This work discusses the different approaches based on real CT scans, and aims to provide advice on the segmentation process for multi-material measurements.

Keywords: Surface determination, segmentation, computed tomography, dimensional metrology, multi-material measurements, INTERAQCT Marie Curie project.

1 Introduction

The use of coordinate measurement systems (CMSs) with the principle of X-ray-based computed tomography (CT) represents a profound change in the field of dimensional metrology. CT allows the inner and outer geometry of mono- or multi-material objects to be measured simultaneously without the need for external access. Besides this, CT provides a favourable information-to-measurement-time ratio, making it possible to perform an extremely large variety of dimensional inspections with just a single scan. These are significant advantages with respect to the classical CMSs when working with soft parts as well as multi-material assemblies. However, today, mono-material measurements are standard and well established in dimensional metrology. Multi-material measurements have emerged recently and need to be critically understood and verified with respect to the additional effects which are part of this more complex measurement.
The benefits of CT have not yet been made fully available to users, due to its high variety of influence factors along the measurement workflow as well as the difficulty of correcting them easily and quickly. Increasing attention is currently being placed on CT post-processing procedures. One objective is to reduce disturbances in image quality, thereby enhancing the accuracy and precision of CT measurements without the need for extending further scanning time or hardware adjustment.
Surface determination is an essential step in the CT post-processing phase for performing dimensional analyses. Without a well-defined surface, it is impossible to fit complex geometric objects (e.g. planes, circles, cylinders, etc.) or just fit single points on the surface, and consequently to perform measurements.
Basically, surface determination consists in defining the contour of objects. Thus, it is intrinsically a segmentation technique. However, surface determination algorithms can be additionally assisted by several kinds of segmentation techniques as a pre-processing step. Segmentation is defined as the process of separating 2D or 3D data into regions, in order to obtain meaningful data for specific tasks [1]. In this paper, segmentation is used as both a surface determination step and a pre-processing step. Segmentation as an optional pre-processing step of surface determination can be used for creating starting surfaces to assist the built-in surface determination algorithms of the software. The two most common surface determination techniques used in dimensional CT are explained below (i.e. the ISO-50% and local threshold methods). Further segmentation techniques applied within the scope of this work are either well known in the image processing field and can be seen in more detail in [1], or are explained in more detail in section 3.2.

The global method of surface determination based on a static threshold value (e.g. ISO-50% as frequently chosen) was the first segmentation algorithm implemented in CT for dimensional metrology. The method works on the overall grey value behaviour of the CT reconstructed volume, and it is usually assumed to be defined as a mean value (i.e. 50 %) between the peaks of the background distribution (i.e. air) and the material distribution (i.e. workpiece). However, there are limitations associated with the global algorithm, for instance, the estimation of the distribution parameters when an overlapping of the distributions occurs. The optimal settings can vary over the workpiece. This implies that only one thresholding value is not sufficient to segment a 3D dataset properly [2]. In addition, artefacts can also be found in the image, which make the task of the surface determination algorithm even more difficult. Beam hardening, noise or other image artefacts corrupt the 3D information, yielding a non-constant grey value in the CT dataset, which can generate an offset of the surface. Therefore, the ISO-50% method is more prone to systematic errors.

Consequently, new and more sophisticated approaches have been developed. The local thresholding method has been developed aiming to segment the dataset locally, providing reliable information even in an artefact-corrupted dataset. Such algorithms allow selecting a threshold for a small group of voxels, while taking into consideration their intensity within a definable bidirectional search distance over a preliminary surface defined by the algorithm [3][4] . This preliminary surface is assumed to be, e.g. obtained from the global threshold. The local accuracy of local thresholding, in a mono-material scenario, may lie within less than 1/10th of a voxel size under optimal conditions [5].

Additionally, further studies concerning surface extraction in CT have been carried out. Ontiveros 2013 et al. [6] analysed different segmentation methods using a tetrahedron as a reference standard, and also implemented and compared a Canny-based method in a 3D dataset with a local threshold method. The Canny-based method presented better repeatability. However, the deviation obtained with the local thresholding method was smaller. Heinzl et al. 2007 [7] compared a series of global and local thresholding methods for dimensional measurement and stated the necessity of sophisticated algorithms for dimensional measurement tasks. The segmentation of multi-material workpieces using a dual-energy CT was presented by [8]. An improvement of the CT results by up to half of the mean deviation using a dual energy CT, compared with a mono CT scan was achieved. On the other hand, Fujimori and Suzuki 2005 [9] presented a new method for extracting surfaces from a dual-material dataset based on voxel classification. A maximum error of the extracted surface of one voxel size was achieved. Shammaa et al. 2010 [10] proposed a combined method of two well-known algorithms (i.e. region growing and graph-cut) for classifying the volumetric model of a multi-material CT dataset. The algorithm works for extracting surfaces of materials that have a high attenuation difference (materials with a large difference concerning X-ray attenuation). However, the method presents some weaknesses in classifying voxels with similar CT values, especially if the dataset is very noisy.

Lifton et al. 2015 [11] studied the uncertainty of surface determination in dimensional CT. The measurement uncertainty due to surface determination is evaluated through the use of a discrete ramp edge model and a Monte Carlo simulation.

Nevertheless, the development of 3D surface determination algorithms for multi-material scenarios has not yet reached fully satisfying results. It becomes clear that the use of one threshold value is not suitable for multi-material scenarios; a pre-processing step or a two-step analysis of the data is very often necessary. Therefore, alternative image segmentation algorithms (e.g. multilevel Otsu segmentation, watershed tools, etc.) are available in commercial CT analysis software (e.g. Simpleware ScanIP Simpleware Ltd., AVIZO® Inspect FEI™). A detailed study of such implementations is necessary.

Although CT presents advantages over the classical CMS sensor technologies, the measurement of multi-material workpieces is still a challenge for CT users. Both, the selection of the CT scanning parameters and the selection of proper surface determination parameters represents two important challenges faced by CT users . The second one is specially critical, once algorithms used in the commercially available softwares remain disclosed source, and in most cases standard CT users do not have access to algorithms in use (i.e. black box-like system). Therefore, the aim of this work is to compare surface determination approaches available within the commercial evaluation software Volume Graphics VGStudio Max 2.2.6. Seven image segmentation approaches, two principal algorithms implemented in the software (ISO-50% and advanced mode) and 5 modifications of the advanced mode were evaluated. One object shape (step gauge) made of 3 different materials was selected and combined to analyse the relationship between X-ray absorption and the accuracy of surface determination on a broader scale. In-material (i.e. measurements performed only within one material of a multi-material assembly) bidirectional length measurements were used as measurands.

2 Analysis of the surface determination influence on dimensional CT measurements

CT scans were performed for different multi-material scenarios. Two different principal surface determination algorithms (ISO-50% and advanced mode) were applied. Additionally, the advanced mode was pre-processed by 5 different segmentation approaches, and finally applied in 3 multi- and 3 mono-material assemblies. Calibrated step gauges were used as reference standards for studying the influence of surface determination on CT measurements. Bidirectional length-based analyses of the step gauge flanks were performed, using the representative point based on a patch. Inner and outer measurands were included in the analysis as well.

2.1 Reference standards

Three calibrated step gauges made of aluminium (AlSiMgMn/ 3.2315/ EN AW-6082 $\rho = 2.830$ g/cm^3, $\alpha_L = 22.9 \cdot 10^{-6} K^{-1}$), polyphenylene sulphide PPS ($\rho = 1.650$ g/cm^3, $\alpha_L = 30 \cdot 10^{-6} K^{-1}$), and polyetheretherketone PEEK ($\rho = 1.310$ g/cm^3, $\alpha_L = 50 \cdot 10^{-6} K^{-1}$), see Figure 1 (a), (b) and (c) respectively, were used to investigate the influence of surface determination when performing multi- as well as mono-material measurements. The step gauges were selected due to the plurality of length measurands available, covering most of the measuring volume used, the similar X-ray penetration lengths for all flanks, and due to the possibility to be calibrated using a tactile CMS with low calibration uncertainty. The step gauges in use have dimensions of 55 mm × 8 mm × 7 mm and feature 11 grooves at 2 mm steps (flatness of the grooves less than 5 µm), and they were designed, developed and manufactured by DTU and are described in more detail in [12].

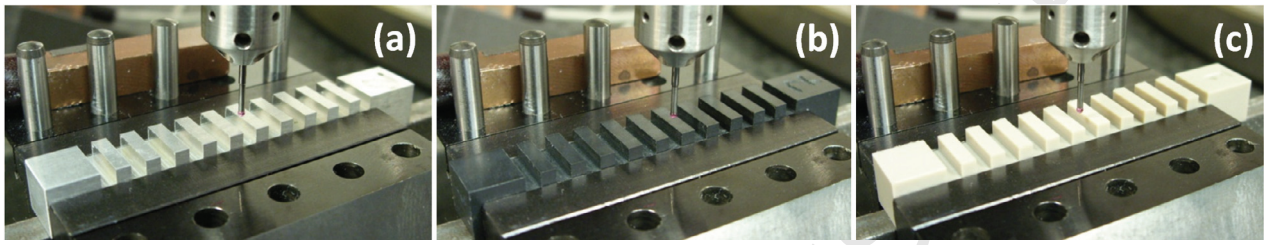

Figure 1. (a) Aluminium, (b) PPS and (c) PEEK step gauges (size 55 mm × 8 mm × 7 mm) designed by DTU [12] and used as reference standards to create assemblies for CT testing.

Reference measurements of the step gauges, using tactile CMS (Carl Zeiss UPMC 850 CARAT) equipped with a ruby probe of 1 mm in diameter, were performed at DTU in a controlled environment of (20±0.5) ºC. Ten bidirectional lengths (6 inner and 4 outer lengths), see Figure 2 (a), were calibrated using substitution method with a traceable step gauge and a patch-based measurement strategy. The traceability of the calibration was established using a step gauge featured by a series of 2-mm gauge blocks used as a reference standard. The patch strategy includes five points distributed in a star-like way along a 2 mm^2 area, centred on the x-axis of the step gauge, see Figure 2 (b). The evaluations were conducted using only the representative points representing the centre of mass of the five fitted points. The patch approach enables more stable results when measuring length by reducing the influence of the sensor noise as well as it improves comparability between CMSs with different sensor technologies, mainly due to the high density of points obtained by CT and to the morphological filtering being present in tactile probing. Furthermore, this calibration approach allows flexibility on the measurands, i.e., it enables the use of single-point- and patch-based measurements. Therefore, comparable measurements between reference and CT measurements can be achieved. Table 1 presents the expanded measurement uncertainty of the reference measurements of the step gauges with the coverage factor k=2.

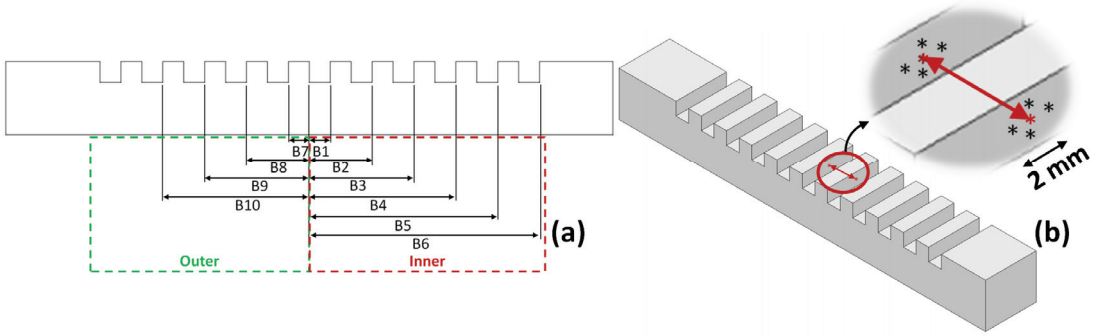

Figure 2. Definition of the measurands (a) inner and outer bidirectional length measurements in the step gauge; (b) patch-based strategy.

	U_{cal} (k=2) in µm
PEEK	1.5
PPS	1.3
Al	1.0

Table 1. Expanded measurement uncertainty of calibrated bidirectional lengths of the step gauges (applicable to all lengths, B1-B10).

2.2 Experimental CT setup

The multi- and mono-material assemblies considered within this work are listed in Table 2. Assemblies 1, 2, and 3 include two step gauges made of different materials, while the remaining assemblies (4, 5 and 6) comprise two step gauges of the same material. The mix of multi-materials enables to map the influence of the multi-material scenarios (assemblies 1, 2 and 3) on a large range of absorption coefficient ratios, while the mono-material scenarios (assemblies 4, 5 and 6) were used as reference.

The assemblies were all positioned tilted at 45º in the PTB's Nikon MCT225 system, see Figure 3 (a), and all scans were performed with the same voxel size of 37 µm. Three repeated scans were performed for each multi- and mono-material assembly using a batch script. A 2D grid-like scaling correction was performed before and after every batch scan to remove residual scaling errors, thus improving the accuracy of the measurements [13]. The temperature in the CT cabin was recorded to be (21 ± 1) ºC and corrections concerning thermal expansion of the measured objects were also performed. Scanning parameters, which are reported in Table 3, were selected for each assembly in such a way as to yield a similar noise level in the multi-material measurements but also to minimize beam hardening effects. The contrast-to-signal ratio (CNR) was used to evaluate the noise [14]. A CNR = 100 ± 10 % for the multi-material scans was achieved in the projections. The grey value profiles of the three multi-material CT scans are plotted in Figure 3 (c), and were obtained from the same slice of the different multi-material CT scans, as shown in Figure 3 (b). For comparability reasons, scanning parameters were unchanged between assemblies 1, 4, and 5, as well as for assemblies 2 and 6, see Table 3. Nikon Metrology CT PRO 3D version 3.1.9 standard software-based noise reduction was carried out during the reconstruction of projections. The settings applied to all of the assemblies evaluated were: Filter type: Hanning, cut off frequency: 100% of maximum frequency, order: 1 and scaling: 1 were used (corresponding to preset 2 of software in use).

	Assembly 1	Assembly 2	Assembly 3	Assembly 4	Assembly 5	Assembly 6
Materials(id_2/id_1)	PEEK/PPS	PPS/Al	PEEK/Al	PEEK/PEEK	PPS/PPS	Al/Al
Density ratio (ρ_2/ρ_1)	0.8	0.6	0.5	1	1	1
Absorption coefficient ratio@150 kV no filter (μ_2/μ_1)	0.4	0.6	0.2	1	1	1

Table 2. Assemblies and their density and absorption coefficient ratios.

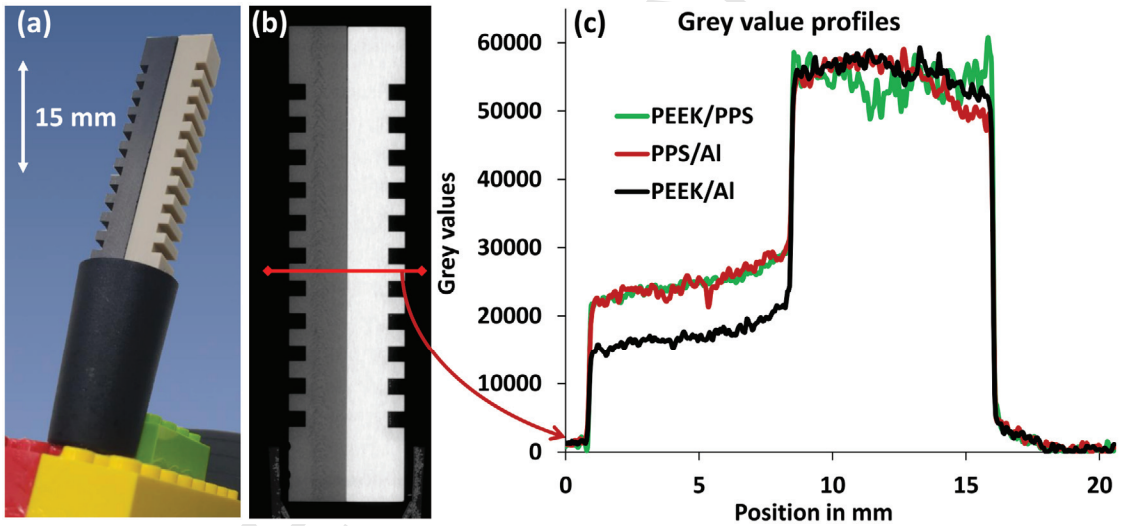

Figure 3. Multi-material assembly, (a) featuring PPS and PEEK as an example; (b) reconstructed vertical CT slice and horizontal profile within this slice where the grey value profile was extracted; (c) plot of the grey value profiles of the three multi-material assemblies.

	Voltage in kV	Current in µA	Filter in mm	No. of projections	Exposure time in ms	Beam hardening correction	Noise reduction (reconstrution filter)
Assembly 1	120	80	Al 0.5	2000	1400	None	Hanning/preset 2
Assembly 2	180	113	Cu 1.5	2000	2829	None	Hanning/preset 2
Assembly 3	170	120	Cu 1.5	2000	2829	None	Hanning/preset 2
Assembly 4	120	80	Al 0.5	2000	1400	None	Hanning/preset 2
Assembly 5	120	80	Al 0.5	2000	1400	None	Hanning/preset 2
Assembly 6	180	113	Cu 1.5	2000	2829	None	Hanning/preset 2

Table 3. CT scanning parameters used for each assembly.

2.3 Evaluation

Evaluations of the different surface determination approaches were based on deviations from tactile CMS reference measurements. Only in-material measurements were considered in this paper (i.e. measurements performed only within one material at a time).

In order to have comparable data, the same alignment procedure and the same measurement strategy were applied in CT and the reference measurements. Patch-based bidirectional measurements were conducted on each step gauge, as shown in

Figure 2. Such choices were made to obtain stable results due to the fact that potential (small) differences between different segmentation approaches may occur. Thus, the use of patches and averaging multiple scans allow the uncertainty to be minimized. Besides this, the results are stabilized with respect to noise and beam hardening effects.
Systematic effects due to the different surface determination methods are of interest in this paper. Each different surface determination approach is evaluated in the same CT dataset (i.e. no new CT scan is performed for each surface determination approach). Thus, the uncertainty of the experiment has to be low enough to make a statement (i.e. a decision).
For the multi-material assemblies, two-step analyses were performed. Surface determination (and segmentation processes) were applied to the higher absorption material (hereafter "HAM") and for the lower absorption material (hereafter "LAM") separately, cf. Table 2. A total of 7 surface determination methods were considered, partly using additional segmentation approaches (in 5 cases). Five surface determination processes were applied to the HAM, 7 to the LAM and 4 surface determination processes to the mono-material scenarios, see Table 4. Several complex surface determination processes were applied. These processes partly used segmentation techniques as pre-processing steps. Potential differences in the approaches were expected and needed to be analysed. A description of each method is presented:

	Multi-material assembly		Mono-material assembly
	HAM	LAM	
The ISO-50% method (ISO)	X	X	X
Advanced (Adv)	X	X	X
Cutting-out + advanced (Cut)	X	X	X
Region growing + advanced (Rgrow)	X	X	X
Histogram-based + advanced (Hist)	X	X	
Subtraction of ROIs + advanced (ROI)		X	
Inversion + advanced (Inv)		X	

Table 4. Test scenarios and surface determination processes under study.

1. The ISO-50% method – ISO (no segmentation step)

ISO-50% is the fastest and simplest segmentation process applied in this study; it uses a static global threshold value based on all voxels present in the volume. For the LAM, the threshold value was selected by means of the automatic selection of the threshold value, available in VG Studio Max; see Figure 4 (a). On the other hand, for the HAM, the threshold value was selected by dragging the "material" line to the maximum of the most right-hand side peak of the histogram, assuming the peak has normal distribution, see Figure 4 (c).
The definition of the surface using the ISO-50% approach and the final CT volumes for the LAM and the HAM are presented in Figure 4 (b) and (d), respectively.

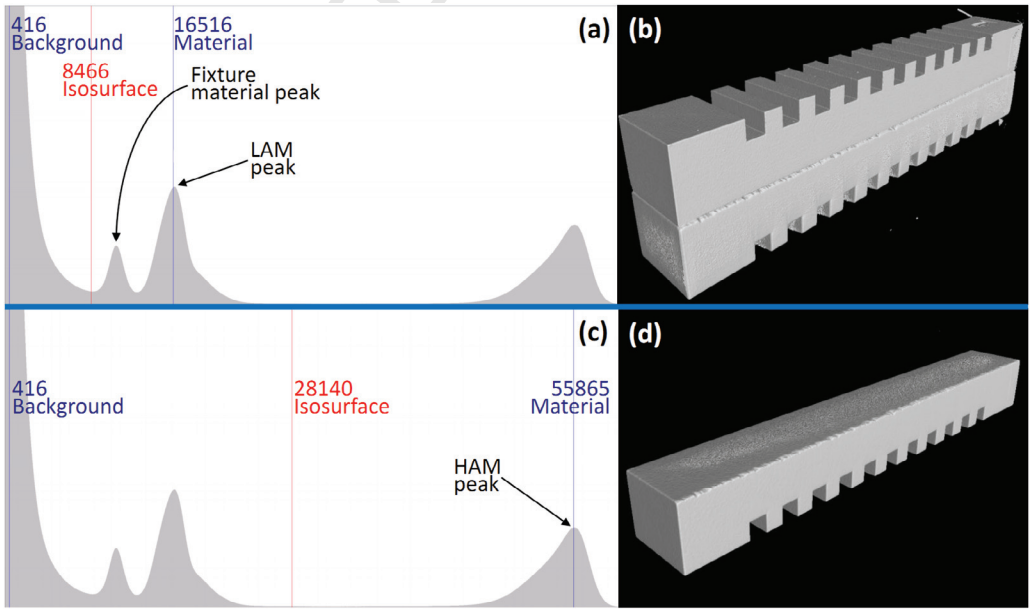

Figure 4. ISO-50% surface determination method (a) histogram presenting the automatic selection of the threshold value for the LAM; (b) CT volume after performing ISO-50% method to the LAM; (c) histogram presenting the manually dragged "material" line to the most right-hand side peak of the histogram; (d) CT volume after performing ISO-50% for the HAM.

Whenever possible the automatic selection of the threshold value was applied. Preliminary studies have shown that the automatic selection of the threshold value presents better results than using the minimum value between the peaks. The automatic selection of the threshold value finds the arithmetic mean value of both background and material distribution, represented by "background" and "material" lines shown in Figure 4 (a). However, in such multi-material scenarios, the automatic selection of the threshold value only applies to the LAM for most of the segmentation methods applied.

2. Advanced method – Adv (no segmentation step)

The advanced mode or local threshold method commonly represents the state-of-the-art tool of 3D surface determination within the software in use. Except for ISO-50%, all the segmentation processes applied in this paper were used in combination with the advanced mode. The following segmentation methods aim to utilize different starting contours and applying the advanced mode for the following surface determination step. The advanced mode surface determination is based on the local behaviour of the grey values, using a starting contour of the object. This starting contour is assumed to be the ISO-50% contour as the software default settings. When applying the advanced mode with no additional segmentation method, the automatic selection of the threshold, i.e. the starting contour, is only possible for the LAM in the scenarios presented in this work. For the HAM, the starting contour is based on the manual drag and drop process of the "material" line to the HAM peak of the histogram as described in the ISO-50% method, see Figure 4 (c). The advanced surface determination parameters were used with the software defaults, e.g. a searching distance of 4 voxels. It is assumed that the searching distance defines the length which the algorithm uses to locally calculate the surface, see Figure 5.

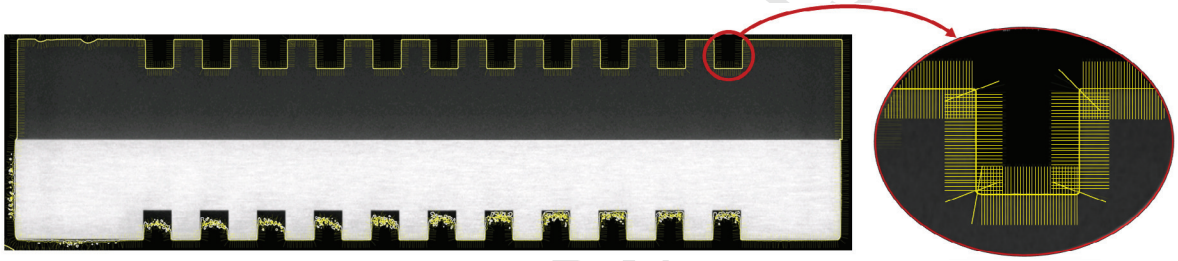

Figure 5. Search distance of the advanced mode.

3. Cutting-out method – Cut (segmentation step)

The cutting-out method is the first segmentation method used prior to the use of the advanced method for surface determination. Cutting out is based on eliminating the "unwanted" material of the scenario (e.g. when measuring the LAM, cut the HAM out). The segmentation of the material is performed using a manually-set rectangle-based region of interest (ROI) as a selection mode in the slice windows. If necessary, a combination of more than one ROI to eliminate "unwanted" materials, e.g. the clamping system, is possible. The cut parts of the volume are filled with void. It appears to be critical that the ROI selection is set manually, due to the fact that too much or too little material may be cut. However, the interface (HAM/LAM interface) is not measured, thus an error in the selection of the ROI has a small influence on the material to be measured. Such a method was applied in order to create a mono-material scenario for the subsequent surface determination step.

4. Region growing method – Rgrow (segmentation step)

The segmentation method based on the region growing process was applied to the material to be measured (independently for the HAM and the LAM). A "seed" has to be "planted" in the middle of the material to be segmented (i.e. far from the material borders). Subsequently, the software adds voxels to the growing region as long as their grey value is within the range of the tolerance value relative to the seed grey value, using the static mode (i.e. the grey value of the seed is constant) [15]. The tolerance value was selected on an empirical basis to be approximately 3 times the standard deviation of the LAM and HAM distribution respectively in the histogram. Finally, the advanced mode of the surface determination is used as well, using the ROI-based region growing method as the starting contour.

5. Histogram-based cut method – Hist (segmentation step)

The histogram-based cut segmentation method aims to exclude the non-desired material distribution from the histogram. The exclusion of the material is performed by disabling a selected range of grey values in the histogram, in the opacity manipulation area palette, centred in the peak of the non-desired material, see Figure 6 (a) and (c). A mono-material scenario is created, and the excluded part of the volume is filled with void, see Figure 6 (b) and (d). For both the LAM and the HAM, the selection range is defined by approximately twice the standard deviation of the distribution. From the enabled part of the histogram, a new volume is extracted and the advanced mode of the surface determination is applied. The surface determination settings are based on the software default. Using this method, there is a risk of creating voids in the material and bubbles in air, especially when the material distributions are too broad or too short. A potential way of overcoming this problem is the use of additional morphological filters (e.g. erosion and dilation, opening and closing as an option available in the software applied). In this paper the use of such filters was not necessary, and therefore, not applied.

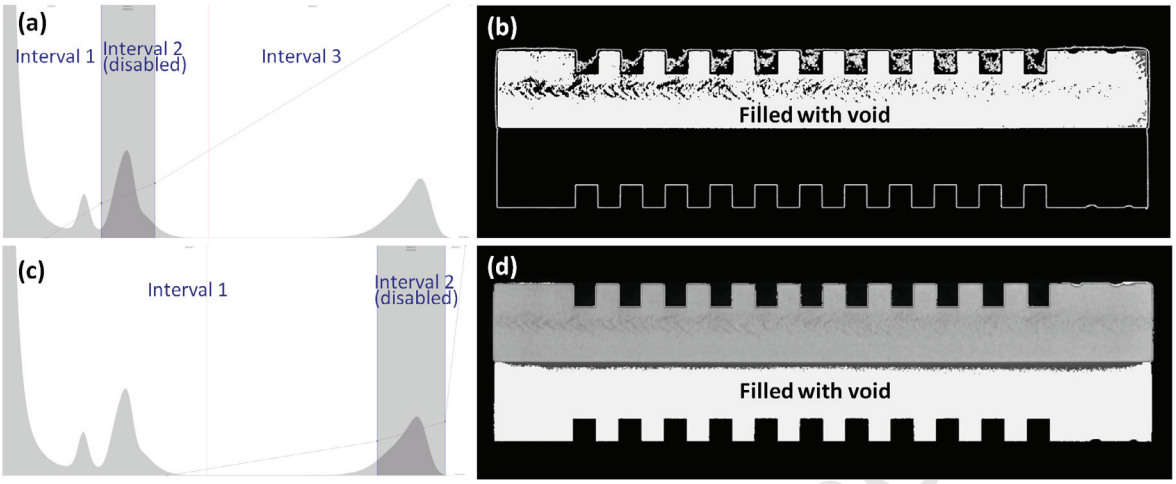

Figure 6. Histogram-based cut method; (a) histogram with the LAM interval disabled; (b) resulting volume with the LAM interval disabled; (c) histogram with the HAM interval disabled; (d) resulting volume with the LAM interval disabled.

6. Subtraction manipulation of ROIs – ROI (this approach only applies to the LAM and uses a segmentation step)

The subtraction manipulation of ROIs tries to obtain only the LAM in the scenario and thus perform the advanced mode surface determination as a mono-material scenario. This method is based on the creation of surface-based ROIs. The advanced mode-based surface is created for the LAM and the HAM in two steps. In the first step, the surface is focused on the LAM, see the ISO-50% method. However, both the LAM and the HAM are presented in the scenario. A ROI based on the common surface is created. In the second step, the surface-based advanced mode focused on the HAM, only the HAM is presented in the scenario. A second ROI based on the surface is created. A ROI containing only the LAM is obtained by subtracting the ROI based on the LAM (containing the LAM and the HAM) with the ROI based on the HAM. Finally, a new advanced surface determination step is performed. However, in this process, the resulting ROI is used as starting a contour.

7. Inverse method – Inv (this approach only applies to the LAM and uses a segmentation step)

The inverse segmentation method aims to obtain the LAM as a mono-material scenario as well. The segmentation is performed by similar means to those performed in the advance method for the HAM. The drag and drop procedure of the "material" line to the most right-hand side peak of the histogram (see Figure 4), using the software default parameter of the searching distance of 4 voxels defines the surface in the HAM. Once the surface is defined, a ROI-based surface is created and an inversion of the ROI, using the manipulation of ROIs, is then performed. A new mono-material volume, containing the LAM and air, is extracted from the inverted ROI. In the new volume, advanced surface determination is applied.

Furthermore, the uncertainty of the experiments by CT was considered in this study taking inspiration from the ISO/TS 23165:2006 standard [16]. The test value uncertainty concept is an approach to evaluate the expanded uncertainty of a test associated solely with the testing equipment and its use in that test. This concept is mainly applied to decision making when performing acceptance testing of a tactile CMS according to the standard ISO 10360-2. Due to the fact that any possible effect which may affect the test is considered and quantified as an uncertainty contributor, the test uncertainty expresses how accurate the testing process is. Nevertheless, the experimental setup presented in this paper represents a similar setup to the test proposed in the ISO 10360-2 standard. Some differences can be observed, e.g. the use of patch-based analyses as a first difference to the standard. The standard uncertainty of the error of indication, $u(E)$, was defined taking inspiration from the ISO/TS 23165 according to Equation 1.

$$u(E) = \sqrt{u^2(\varepsilon_{cal}) + u^2(\varepsilon_{\alpha}) + u^2(\varepsilon_t) + u^2(\varepsilon_{align}) + u^2(\varepsilon_{fixt}) + u^2(\varepsilon_{rep})} \quad (1)$$

where:

ε_{cal} is the calibration error of the reference standard
ε_{α} is the error due to the input value of the CTE of the reference standard
ε_t is the error due to the input value of the temperature of the reference standard
ε_{align} is the error due to misalignment of the reference standard
ε_{fixt} is the error due to fixturing of the reference standard
ε_{rep} is the repeatability of the three repeated measurements by CT

$u(\varepsilon_{cal})$ is directly obtained by the reference measurements of the step gauges, divided by the coverage factor, see Table 1. The CTE value was obtained from the manufacturer datasheet and the uncertainty of the CTE value is often unknown. In this case,

the guideline VDI/VDE/DGQ 2618 part 1.2:2003-12, could be followed, where a minimal range of 20 % of the nominal value should be used as a rectangular distribution [17]. However, there is only a small contribution due to the CTE error (ε_α), thus it can be neglected. The ε_t contribution is usually zero in all relevant cases in acceptance testing [16]. The influence of the uncertainty of the temperature is attributed to the tactile CMS data in standard testing (i.e. the ε_t contribution is zero). However, in the experiments presented in this paper, a change in the temperature caused an expansion of the workpiece, which impaired the results. Therefore, based on out of date reference measurements of the temperature sensor and the knowledge of an expert user, the uncertainty due to (ε_t) was estimated at 0.2 µm. $u(\varepsilon_{align})$ was checked by applying the same alignment procedure and measuring lengths three times in the same dataset; raw CT data was used every time. A range of 0.3 µm was observed. Assuming rectangular distribution, the error due to the alignment procedure was considered $u(\varepsilon_{align})$= 0.17 µm. For the $u(\varepsilon_{fixt})$, no significant effect was considered due to the fact that no significant clamping force was used. Finally, the repeatability of the three consecutive CT scans, $u(\varepsilon_{rep})$, was considered as well. This is a second difference to the ISO/TC 23165 standard, which does not consider repeatability. However, with bad repeatability, no statement of the effects can be made. The biggest standard deviation, obtained by the three consecutive measurements by CT, divided by the square root of 3 characterizes $u(\varepsilon_{rep})$. ε_{cal} and ε_{rep} were the biggest error sources observed in this study.
The expanded uncertainties were quantified for the HAM and for the LAM in each multi-material assembly. The respective expanded uncertainties with a coverage factor k = 2 of each step gauge on each assembly are presented in Table 5.

	U_L^{CT} (k=2) in µm	
LAM/HAM	**LAM**	**HAM**
PEEK/PPS	2.2	2.0
PPS/Al	2.0	3.0
PEEK/Al	3.0	2.6
PEEK/PEEK	2.3	
PPS/PPS	2.2	
Al/Al	1.9	

Table 5. Average expanded uncertainty of patch-based bidirectional CT length measurements of PEEK, PPS and Al step gauges on each mono- and multi-material assembly (HAM: higher absorption material, LAM: lower absorption material).

3 Results

CT datasets obtained with different multi- and mono-material scenarios and different segmentation methods in combination with two main surface determination algorithms were tested. In-material bidirectional length measurements using a patch operator were carried out in step gauges as reference standards.
The results of the dimensional evaluation allow the investigation of whether there is an influence of the different segmentation methods as well as the multi-material scenarios on the measurements. The results of the multi- and mono-material assemblies are presented in Figure 7 and Figure 8, respectively. Red words in the headings of the graphs indicate the measured material. In general, considering the experiment uncertainty applied in this study (represented as bars in the graphical results), no significant influence concerning the different segmentation methods, except for ISO-50% method, was observed for most of the results. For simplicity reasons, the uncertainty bars were represented only in the average value of two segmentation methods. A maximum measurement error of 40 % of the voxel size (i.e. 15 µm) for all of the applied segmentation methods, except for the ISO-50%, was observed. For the ISO-50% method, the maximum measurement error is nearly 1 voxel size (32 µm). Measurement error is characterised by the difference between the measured and calibrated values.
Concerning the multi-material influence on the measurements, an effect of the measurement error behaviour being dominated by the HAM was observed. Figure 7 (b) and (f) depicts PEEK measurements in the presence of PPS and Al, respectively. The measurement error behaviour is similar for both measurements, once the PEEK is the lighter material in both scenarios. However, a slightly broader range of the segmentation methods could be observed in the PEEK/Al case, which can be explained by the fact that Al is heavier than PPS. This means, when performing measurements of the LAM (i.e. surface determination focused on the LAM) in a multi-material scenario, the error behaviour on the LAM will be negatively affected by the HAM.
The error behaviour dominated by the HAM is confirmed by the PPS measurements. Figure 7 (d) depicts an improvement of the measurement error when compared with the PEEK/PPS scenario; see Figure 7 (a).
Furthermore, a similar behaviour of the PPS measurements can be observed when comparing PEEK/PPS and PPS/PPS scenarios, see Figure 7 (a) and Figure 8 (b). However, slightly worse behaviour in the PPS/PPS measurement when compared to PEEK/PPS was observed. This can be explained by the fact that PPS is heavier than PEEK and the same scanning parameters were used for both scans. The dominance of the HAM effect was also confirmed by the measurements of Al, as this material is the highest absorption material considered in this study. In the aluminium measurements, the error behaviour was similar for both cases in the presence of a second lighter material, see Figure 7 (c), (e) and Figure 8 (c). This means, when performing a measurement of the HAM (i.e. surface determination focused on the HAM) in multi-material scenarios, only a small influence of the LAM on the HAM can be observed.

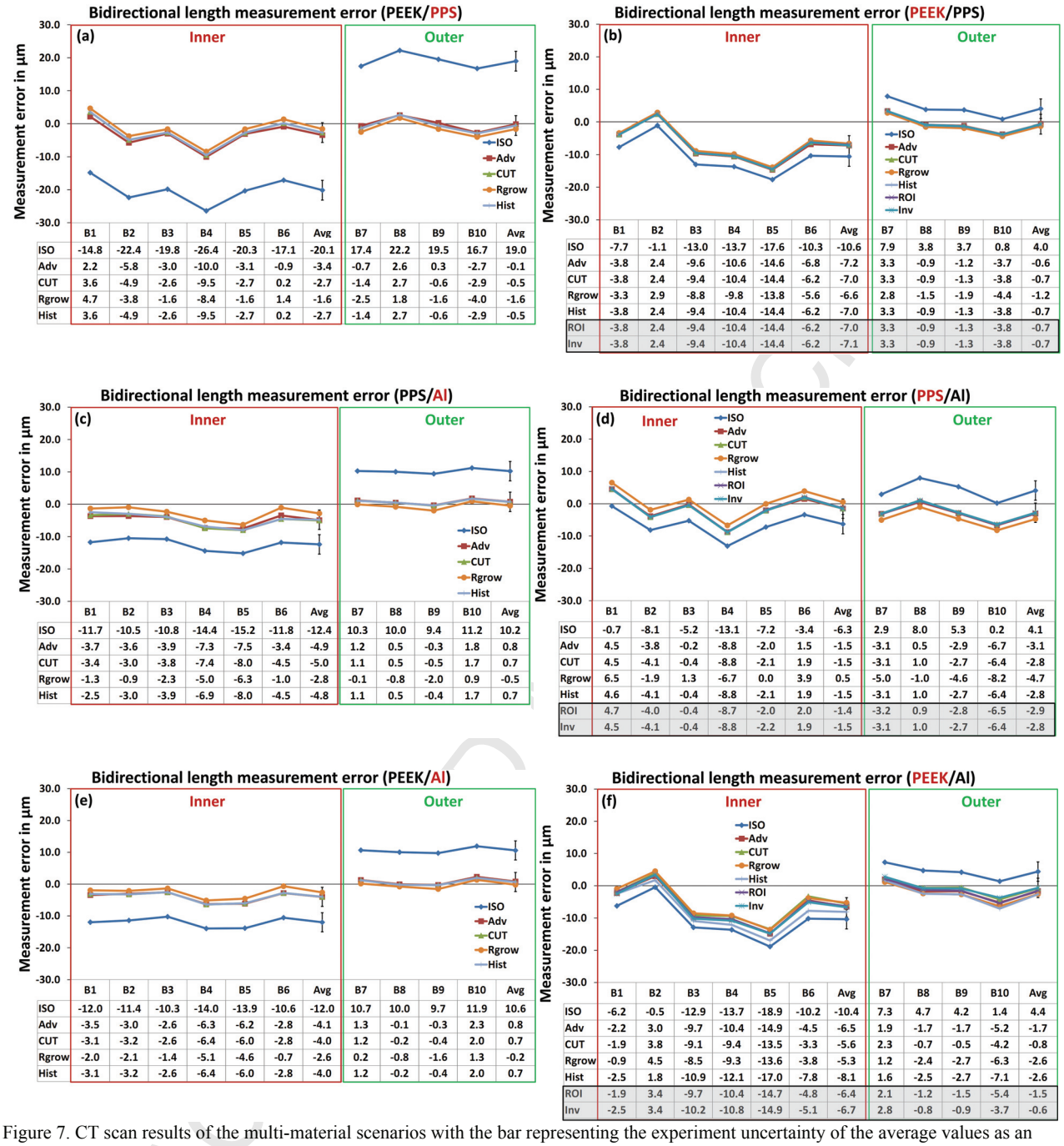

	B1	B2	B3	B4	B5	B6	Avg	B7	B8	B9	B10	Avg
ISO	-14.8	-22.4	-19.8	-26.4	-20.3	-17.1	-20.1	17.4	22.2	19.5	16.7	19.0
Adv	2.2	-5.8	-3.0	-10.0	-3.1	-0.9	-3.4	-0.7	2.6	0.3	-2.7	-0.1
CUT	3.6	-4.9	-2.6	-9.5	-2.7	0.2	-2.7	-1.4	2.7	-0.6	-2.9	-0.5
Rgrow	4.7	-3.8	-1.6	-8.4	-1.6	1.4	-1.6	-2.5	1.8	-1.6	-4.0	-1.6
Hist	3.6	-4.9	-2.6	-9.5	-2.7	0.2	-2.7	-1.4	2.7	-0.6	-2.9	-0.5

	B1	B2	B3	B4	B5	B6	Avg	B7	B8	B9	B10	Avg
ISO	-7.7	-1.1	-13.0	-13.7	-17.6	-10.3	-10.6	7.9	3.8	3.7	0.8	4.0
Adv	-3.8	2.4	-9.6	-10.6	-14.6	-6.8	-7.2	3.3	-0.9	-1.2	-3.7	-0.6
CUT	-3.8	2.4	-9.4	-10.4	-14.4	-6.2	-7.0	3.3	-0.9	-1.3	-3.8	-0.7
Rgrow	-3.3	2.9	-8.8	-9.8	-13.8	-5.6	-6.6	2.8	-1.5	-1.9	-4.4	-1.2
Hist	-3.8	2.4	-9.4	-10.4	-14.4	-6.2	-7.0	3.3	-0.9	-1.3	-3.8	-0.7
ROI	-3.8	2.4	-9.4	-10.4	-14.4	-6.2	-7.0	3.3	-0.9	-1.3	-3.8	-0.7
Inv	-3.8	2.4	-9.4	-10.4	-14.4	-6.2	-7.1	3.3	-0.9	-1.3	-3.8	-0.7

	B1	B2	B3	B4	B5	B6	Avg	B7	B8	B9	B10	Avg
ISO	-11.7	-10.5	-10.8	-14.4	-15.2	-11.8	-12.4	10.3	10.0	9.4	11.2	10.2
Adv	-3.7	-3.6	-3.9	-7.3	-7.5	-3.4	-4.9	1.2	0.5	-0.3	1.8	0.8
CUT	-3.4	-3.0	-3.8	-7.4	-8.0	-4.5	-5.0	1.1	0.5	-0.5	1.7	0.7
Rgrow	-1.3	-0.9	-2.3	-5.0	-6.3	-1.0	-2.8	-0.1	-0.8	-2.0	0.9	-0.5
Hist	-2.5	-3.0	-3.9	-6.9	-8.0	-4.5	-4.8	1.1	0.5	-0.4	1.7	0.7

	B1	B2	B3	B4	B5	B6	Avg	B7	B8	B9	B10	Avg
ISO	-0.7	-8.1	-5.2	-13.1	-7.2	-3.4	-6.3	2.9	8.0	5.3	0.2	4.1
Adv	4.5	-3.8	-0.2	-8.8	-2.0	1.5	-1.5	-3.1	0.5	-2.9	-6.7	-3.1
CUT	4.5	-4.1	-0.4	-8.8	-2.1	1.9	-1.5	-3.1	1.0	-2.7	-6.4	-2.8
Rgrow	6.5	-1.9	1.3	-6.7	0.0	3.9	0.5	-5.0	-1.0	-4.6	-8.2	-4.7
Hist	4.6	-4.1	-0.4	-8.8	-2.1	1.9	-1.5	-3.1	1.0	-2.7	-6.4	-2.8
ROI	4.7	-4.0	-0.4	-8.7	-2.0	2.0	-1.4	-3.2	0.9	-2.8	-6.5	-2.9
Inv	4.5	-4.1	-0.4	-8.8	-2.2	1.9	-1.5	-3.1	1.0	-2.7	-6.4	-2.8

	B1	B2	B3	B4	B5	B6	Avg	B7	B8	B9	B10	Avg
ISO	-12.0	-11.4	-10.3	-14.0	-13.9	-10.6	-12.0	10.7	10.0	9.7	11.9	10.6
Adv	-3.5	-3.0	-2.6	-6.3	-6.2	-2.8	-4.1	1.3	-0.1	-0.3	2.3	0.8
CUT	-3.1	-3.2	-2.6	-6.4	-6.0	-2.8	-4.0	1.2	-0.2	-0.4	2.0	0.7
Rgrow	-2.0	-2.1	-1.4	-5.1	-4.6	-0.7	-2.6	0.2	-0.8	-1.6	1.3	-0.2
Hist	-3.1	-3.2	-2.6	-6.4	-6.0	-2.8	-4.0	1.2	-0.2	-0.4	2.0	0.7

	B1	B2	B3	B4	B5	B6	Avg	B7	B8	B9	B10	Avg
ISO	-6.2	-0.5	-12.9	-13.7	-18.9	-10.2	-10.4	7.3	4.7	4.2	1.4	4.4
Adv	-2.2	3.0	-9.7	-10.4	-14.9	-4.5	-6.5	1.9	-1.7	-1.7	-5.2	-1.7
CUT	-1.9	3.8	-9.1	-9.4	-13.5	-3.3	-5.6	2.3	-0.7	-0.5	-4.2	-0.8
Rgrow	-0.9	4.5	-8.5	-9.3	-13.6	-3.8	-5.3	1.2	-2.4	-2.7	-6.3	-2.6
Hist	-2.5	1.8	-10.9	-12.1	-17.0	-7.8	-8.1	1.6	-2.5	-2.7	-7.1	-2.6
ROI	-1.9	3.4	-9.7	-10.4	-14.7	-4.8	-6.4	2.1	-1.2	-1.5	-5.4	-1.5
Inv	-2.5	3.4	-10.2	-10.8	-14.9	-5.1	-6.7	2.8	-0.8	-0.9	-3.7	-0.6

Figure 7. CT scan results of the multi-material scenarios with the bar representing the experiment uncertainty of the average values as an example. In the headings of the charts, red words indicate the measured material. Bidirectional length measurement error on the assemblies PEEK/PPS, (a) measured in PPS and (b) measured in PEEK; PPS/Al, (c) measured in Al and (d) measured in PPS; PEEK/Al, (e) measured in Al and (f) measured in PEEK. Cf. Figure 2 for lengths and Table 4 for methods.

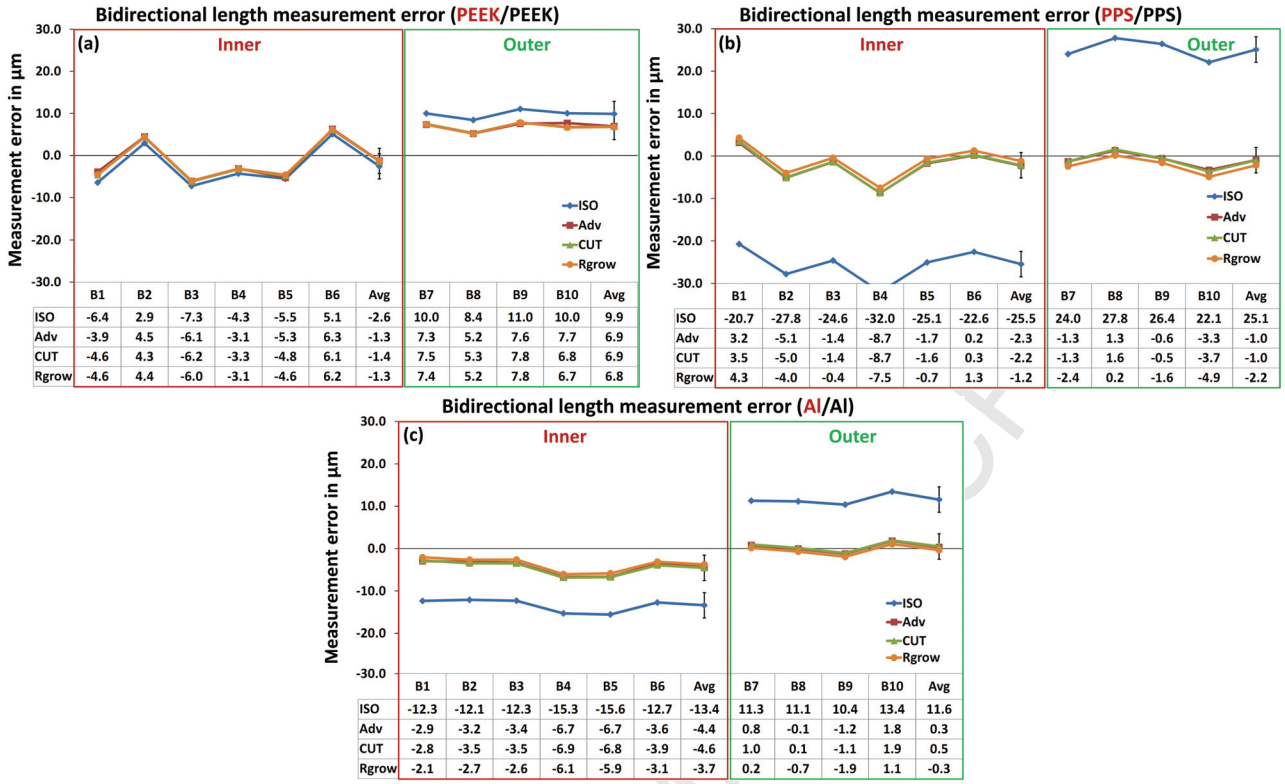

(a) PEEK/PEEK	B1	B2	B3	B4	B5	B6	Avg	B7	B8	B9	B10	Avg
ISO	-6.4	2.9	-7.3	-4.3	-5.5	5.1	-2.6	10.0	8.4	11.0	10.0	9.9
Adv	-3.9	4.5	-6.1	-3.1	-5.3	6.3	-1.3	7.3	5.2	7.6	7.7	6.9
CUT	-4.6	4.3	-6.2	-3.3	-4.8	6.1	-1.4	7.5	5.3	7.8	6.8	6.9
Rgrow	-4.6	4.4	-6.0	-3.1	-4.6	6.2	-1.3	7.4	5.2	7.8	6.7	6.8

(b) PPS/PPS	B1	B2	B3	B4	B5	B6	Avg	B7	B8	B9	B10	Avg
ISO	-20.7	-27.8	-24.6	-32.0	-25.1	-22.6	-25.5	24.0	27.8	26.4	22.1	25.1
Adv	3.2	-5.1	-1.4	-8.7	-1.7	0.2	-2.3	-1.3	1.3	-0.6	-3.3	-1.0
CUT	3.5	-5.0	-1.4	-8.7	-1.6	0.3	-2.2	-1.3	1.6	-0.5	-3.7	-1.0
Rgrow	4.3	-4.0	-0.4	-7.5	-0.7	1.3	-1.2	-2.4	0.2	-1.6	-4.9	-2.2

(c) Al/Al	B1	B2	B3	B4	B5	B6	Avg	B7	B8	B9	B10	Avg
ISO	-12.3	-12.1	-12.3	-15.3	-15.6	-12.7	-13.4	11.3	11.1	10.4	13.4	11.6
Adv	-2.9	-3.2	-3.4	-6.7	-6.7	-3.6	-4.4	0.8	-0.1	-1.2	1.8	0.3
CUT	-2.8	-3.5	-3.5	-6.9	-6.8	-3.9	-4.6	1.0	0.1	-1.1	1.9	0.5
Rgrow	-2.1	-2.7	-2.6	-6.1	-5.9	-3.1	-3.7	0.2	-0.7	-1.9	1.1	-0.3

Figure 8. CT scan results of the mono-material scenarios with the bar representing the experiment uncertainty of the average values as an example. In the headings of the charts, red words indicate the measured material. Bidirectional length measurement error on the assemblies (a) PEEK/PEEK; (b) PPS/PPS; and (c) Al/Al, cf. Figure 2 for lengths and Table 4 for methods.

4. Conclusion and summary

Step gauges made of aluminium, PEEK and PPS were used as reference standards to study the surface determination influence on in-material length measurements in multi-material scenarios. Reference measurements of the step gauges were carried out with a tactile CMS and the CT results were compared with the reference values.

For the CT measurements, mono- and multi-material step gauge assemblies were scanned, providing a broader range in the attenuation coefficient ratio. Three repeated measurements of each assembly were performed and considered in the uncertainty budget performed in this paper.

Inspired by the test value uncertainty standard ISO/TS 23165, a study of the CT experiment uncertainty was part of the scope of this research, considering the most important influence factors of the experiment (e.g. repeatability, reference standards calibration uncertainty).

ISO-50% and local threshold surface determination algorithms were applied in mono- and multi-material scenarios. However, it is not possible to measure two materials using only one threshold value for the multi-material case. Therefore, one threshold value for the HAM and one threshold value for the LAM, as well as different segmentation methods available in VGStudio Max 2.2.6 were used in this study. The different segmentation methods worked as a pre-processing step of the local threshold surface determination algorithm.

In-material bidirectional length measurements using a patch operator were performed in multi- and mono-material assemblies. In general, for the length measurements, no significant difference was observed for the different surface determination methods, except for ISO-50%, which presented worse results compared to the others, as expected. However, it is presumed that with an increase of the noise level, larger differences of the different segmentation methods will occur, as the noise of the CT scans was normalized at a low level. For all of the CT scans and segmentation approaches, except ISO-50%, a maximum measurement error of 40 % of the voxel size was achieved. For ISO-50%, the measurement error of nearly 1 voxel size was achieved.

The measurement error behaviour, in the multi-material assemblies, is moreover dominated by the HAM. This means that the HAM influences the measurements of the LAM. On the other hand, the LAM does not significantly affect the HAM measurements. In addition, a decrease of the measurement error was caused by the HAM, when measuring the LAM in a multi-material scenario.

To summarize, the state-of-the-art surface determination algorithm (local threshold method in the software in use) presented stable results with a low measurement error. Although, no significant difference regarding the different segmentation methods as a pre-processing step to local threshold methods was observed, it is expected that segmentation methods will improve the

measurement results when a higher level of noise is found in the CT volume data. Therefore, if the noise level is relatively low, no further segmentation process is necessary. The use of the local threshold method (the advance mode) is sufficient. On the other hand, if the level of noise is relatively high, testing different segmentation methods presented here, e.g. the region growing method, may be suggested.
An extension of this work might be inter-material measurements in multi-material scenarios, which is currently under discussion.
Additionally, this paper can be seen as a contribution to future multi-material acceptance testing which is being developed at present.
The paper is a collaborative work between PTB (Germany) and DTU (Denmark) within the EU Marie Curie INTERAQCT project (FP7-PEOPLE-2013-ITN, grant no.: 607817); see http:\\www.interaqct.eu.

Acknowledgements

We would like to thank the EU Marie Curie Initial Training Networks (ITN) − INTERAQCT, grant agreement no.: 607817, for the project funding. More information can be seen on http//:www.interaqct.eu.
We would also like to express our gratitude to our colleagues Rene Sobiecki (DTU) for the discussions and advice concerning the reference measurements of the step gauges, along with Jens Illemann and Olga Kazankova (PTB) for their assistance with the scaling factor correction application.

References

[1] B.M. Dawant, A. P. Zijdenbos, Image segmentation in: M. Sonka, J.M. Fitzpatrick (Eds.), Handbook medical imaging: Volume 2. Medical image processing and analysis, SPIE Press, Washington, 2000, pp. 71-127
[2] Y. Tan, K. Kiekens, J.P. Kruth, A. Voet, W. Dewulf, Material dependent thresholding for dimensional X-ray computed tomography, Intern. symp. on digital industrial radiology and computed tomography, Berlin, June 2011
[3] H. Steinbeiss, Verfahren und Vorrichtung zur Konturfeinermittlung eines Objekts bei bildgebenden Untersuchungsverfahren, Europäische Patentschrift, EP 1 861 822 B1, 2011
[4] H. Lettenbauer, A. Lotze, S. Kunzmann, Method and device for indentifying material bounderies of a test object, US Patent US 8,045,806 B2, 2011
[5] C. Reinhart, Industrial computer tomography - A universal inspection tool, Proceedings of the 17th World Conference on Nondestructive Testing (WCNDT), Shanghai, October 2008
[6] S. Ontiveros, J.A. Yagüe, R. Jiménez, F. Brosed, Computer tomography 3D edge detection comparative for metrology applications, Proc. of the 5th Manufacturing engineering society international conference, Zaragoza, June 2013
[7] C. Heinzl, J. Kastner, B. Georgi, H. Lettenbauer, Comparison of surface detection methods to evaluate cone beam computed tomography data for three dimensional metrology, Intern. symp. on digital industrial radiology and computed tomography, Lyon, June 2007
[8] C. Heinzl, J. Kastner, E. Gröller, Surface extraction from multi-material components for metrology using dual energy CT, IEEE transactions on visualization and computer graphics, Vol. 13, No. 6, (2007) pp. 1520-1527
[9] T. Fujimori, H. Suzuki, Surface Extraction from Multi-material CT Data, 9th International conference on computer aided design and computer graphics, Hong Kong, December 2005
[10] M.H. Shammaa, Y. Ohtake, H. Suzuki, Segmentation of multi-material CT data of mechanical parts for extracting boundary surfaces, Computer-Aided Design 42 (2010) pp 118-128
[11] J.J. Lifton, A.A. Malcolm, J.W. McBride, On the uncertainty of surface determination in X-ray computed tomography for dimensional metrology, Measurement Science and Technology, Vol. 26, No. 3 (2015)
[12] J. Angel, L. De Chiffre, J.P. Kruth, Y. Tan, W. Dewulf, Performance evaluation of CT measurements made on step gauges using statistical methodologies, CIRP Journal of Manufacturing Science and Technology, Vol. 11, (2015) pp. 68–72
[13] J. Illemann, M. Bartscher, U. Neuschaefer-Rube, An efficient procedure for traceable dimensional measurements and the characterization of industrial CT systems, Digital Industrial Radiology and Computed Tomography, Ghent, 2015
[14] K. M. Hanson, Detectability in computed tomographic images, Medical Physics 6(5), (1979) pp 441-451
[15] Volume Graphics GmbH, VG Studio Max 2.2 Reference Manual, Heidelberg, 2013.
[16] ISO/TS 23165:2006, Geometrical product specifications (GPS) - Guidelines for the evaluation of coordinate measuring machine (CMM) test uncertainty. International Organization for Standardization, Geneva, 2006
[17] VDI/VDE/DGQ 2618 part 1.2:2003-12, Inspection of measuring and test equipment - Instructions for the inspection of measuring and test equipment for geometrical quantities - Uncertainty of measurement, Düsseldorf, 2003.